Science of the Total Environment 502 (2015) 537–547

Contents lists available at ScienceDirect

Science of the Total Environment

journal homepage: www.elsevier.com/locate/scitotenv

# On the feasibility of measuring urban air pollution by wireless distributed sensor networks

Sharon Moltchanov, Ilan Levy, Yael Etzion, Uri Lerner, David M. Broday *, Barak Fishbain

*The Technion Center of Excellence in Exposure Science and Environmental Health, Faculty of Civil and Environmental Engineering, Technion — Israel Institute of Technology, Haifa 32000, Israel*

## HIGHLIGHTS

- Air quality wireless distributed sensor network was deployed at a sub-neighborhood scale.
- High inter-nodal consistency was demonstrated.
- The nodes were sensitive to local microenvironment conditions and to "hot-spots".
- In-situ calibration procedures for $O_3$ were demonstrated.
- This technology has a great potential for exposure assessment.

## GRAPHICAL ABSTRACT

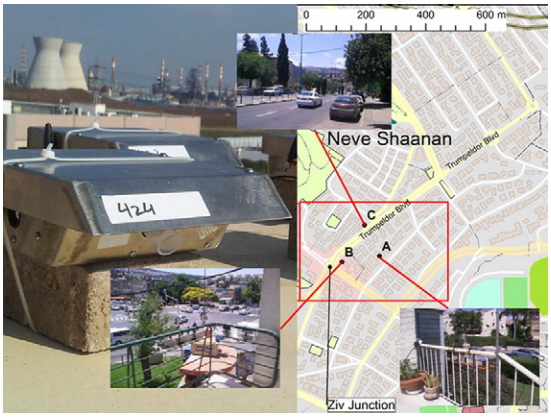


## ARTICLE INFO

*Article history:*
Received 9 April 2014
Received in revised form 17 September 2014
Accepted 19 September 2014
Available online 6 October 2014

Editor: Lidia Morawska

*Keywords:*
Urban air pollution
Exposure
Air quality monitoring
Wireless distributed sensor network

## ABSTRACT

Accurate evaluation of air pollution on human-wellbeing requires high-resolution measurements. Standard air quality monitoring stations provide accurate pollution levels but due to their sparse distribution they cannot capture the highly resolved spatial variations within cities. Similarly, dedicated field campaigns can use tens of measurement devices and obtain highly dense spatial coverage but normally deployment has been limited to short periods of no more than few weeks. Nowadays, advances in communication and sensory technologies enable the deployment of dense grids of wireless distributed air monitoring nodes, yet their sensor ability to capture the spatiotemporal pollutant variability at the sub-neighborhood scale has never been thoroughly tested. This study reports ambient measurements of gaseous air pollutants by a network of six wireless multi-sensor miniature nodes that have been deployed in three urban sites, about 150 m apart. We demonstrate the network's capability to capture spatiotemporal concentration variations at an exceptional fine resolution but highlight the need for a frequent in-situ calibration to maintain the consistency of some sensors. Accordingly, a procedure for a field calibration is proposed and shown to improve the system's performance. Overall, our results support the compatibility of wireless distributed sensor networks for measuring urban air pollution at a sub-neighborhood spatial resolution, which suits the requirement for highly spatiotemporal resolved measurements at the breathing-height when assessing exposure to urban air pollution.



* Corresponding author. Tel.: +972 4 829 3468; fax: +972 4 822 8898.
*E-mail address:* dbroday@tx.technion.ac.il (D.M. Broday).

http://dx.doi.org/10.1016/j.scitotenv.2014.09.059
0048-9697/

## 1. Introduction

Ambient air pollution results from emissions of diverse pollutants from different stationary and mobile sources, and from chemical reactions between primary pollutants that form secondary pollutants, such as tropospheric ozone. The dispersion and the generation of ambient pollutants are highly affected by local (micro-) meteorological conditions (wind speed, solar radiation, humidity, temperature). Accordingly, urban air quality is characterized by high spatial and temporal variability (Nazaroff and Alvarez-Cohen, 2001; Levy et al., 2014a,b).

Evidences of adverse health effects from exposure to ambient gaseous pollutants (e.g. ozone, $O_3$; nitrogen dioxide, $NO_2$; carbon monoxide, CO) and particulate matter (PM) have been widely reported (Kampa and Castanas, 2008; Peters et al., 1997). Typically, air pollution related exposure metrics used in environmental epidemiology studies are based either on short term sampling (Crouse et al., 2009) or on pollutant measurements by standard air quality monitoring (AQM) stations over extended time periods (Pope et al., 2002). Conventional AQM instruments provide accurate measurements but suffer from limited deployment due to their bulkiness, high cost and the professional maintenance requirements. This limits the AQM network capability to adequately capture the highly resolved air pollutant spatial variations. Intensive sampling campaigns use a large number of sensors deployed at high density but are limited to relatively short periods (~14 days), and oftentimes to integrative measurement over the whole period (Hoek et al., 2008). Consequently, accurate exposure assessment and the study of air pollution-health associations are still a challenging task (Rao et al., 2012). To tackle these limitations, recent environmental health studies incorporated proxy indicators of personal exposure to traffic related air pollution, such as distance of the residence to the nearby road (Pujades-Rodríguez et al., 2009) and other land use parameters (Hoek et al., 2008). Yet, the relationships between these surrogates and the individual's exposure are mostly stationary and depend on the choice of variables that are included in model (in part, based on data availability). Exposure estimation based on geospatial interpolation techniques that generate pollution maps from AQM data is also common (Whitworth et al., 2011; Eitan et al., 2010; Myers et al., 2013). However, these methods are dramatically affected by the stations' location (Yuval and Broday, 2006). Clearly, increasing the spatial density of the measurements will result in spatial interpolation with smaller uncertainty (Kanaroglou et al., 2005) but can be economically feasible only by deployment of low-cost instruments. Yet, such low-cost devices may suffer from poor accuracy, lack of robustness, and limited longevity, thus projecting on their deployment flexibility and on the network scaling up.

Recent advances in sensory and communications technologies have made the deployment of multi-sensor environmental wireless distributed sensor networks (WDSNs) feasible, and opened a new front in the air pollution and exposure assessment arena. Early studies that evaluated WDSN capabilities in a controlled lab environment (Lee, 2001; Becker et al., 2000) stressed the need for a calibration process in order to sustain reliable measurements. Field deployments of low-cost air quality sensor networks measuring ambient $O_3$ levels by metal-oxide micro-sensors (Williams et al., 2013) and CO, NO and $NO_2$ by electrochemical (Mead et al., 2013) or metal-oxide (Piedrahita et al., 2014) probes proposed calibration processes that are applicable for controlled lab environment but fell short in comparison to data collected at a collocated standard AQM station (even after an initial field calibration has been applied; Williams et al., 2013). Tsujita et al. (2005) suggested a field calibration approach where the metal-oxide $NO_2$ sensor baseline is adjusted to the average value of four surrounding AQM stations during time periods in which the $NO_2$ concentrations are low (<10 ppb) and homogeneous conditions apply. Yet, the method is designed to work on low $NO_2$ concentrations whereas the WDSN $NO_2$ detection limit is typically 10 ppb. This renders the method inapplicable. Moreover, this calibration method has been tested only on one sensor and has never been applied to a WDSN. To date, testing the operation of an air quality WDSN (AQ-WDSN) in the field has been reported only by Mead et al. (2013), who demonstrated the feasibility of deployment of an electrochemical sensor network. However, a detailed analysis of the network ability to capture the spatiotemporal pollutant variability, micro-environmental conditions (local sources and meteorology effects), and the unavoidable field calibration process has not been performed. Moreover, to the best of our knowledge field deployment of a metal-oxide micro-sensor network has not yet been reported.

This paper presents an analysis of measurements obtained by an AQ-WDSN. The network was deployed in an inner-city neighborhood, with a typical mixture of quiet residential areas, busy traffic routes, a neighborhood commercial area, education institutions, etc. Each node contained multiple sensors, however in this work we focus on measurements of $O_3$, $NO_2$, and total volatile organic compounds (TVOCs). The study aims were to examine the suitability of metal-oxide sensor network for measuring pollutant levels and capturing their spatiotemporal concentration variability, and to develop a reliable field calibration procedure for the sensors.

## 2. Materials and methods

### 2.1. Instrumentation

Air quality measurements were acquired using the CanarIT™ multi-sensor WDSN nodes (Airbase Systems LTD, Israel). Each CanarIT™ unit hosts in a compact housing ($20 \times 15 \times 7$ cm$^3$) three metal oxide (MO) chemoresistive sensors for $O_3$, $NO_2$ and TVOC, an optical (IR based) total suspended particulate matter (TSP) sensor, an electret microphone (noise sensor) and a dual semiconductor temperature and relative humidity (RH) sensor. In this study we discuss only measurements of $NO_2$ and TVOC (taken every 20 s) and $O_3$ (recorded once per minute). The data are sent by a GPRS communications channel to cloud storage.

The $O_3$ sensor (SM50, Aeroqual LTD, New Zealand) is pre-calibrated to the range of 0–150 ppb, and has a 1 ppb resolution and laboratory measurement uncertainty of less than $\pm 5$ ppb. The $NO_2$ and TVOC sensors (iAQ-100, AppliedSensors GmbH, Germany) are pre-calibrated to 10–2000 ppb ($NO_2$, 5 ppb resolution) and 0–2000 ppm $CO_2$ equivalent (TVOC). Ambient pollutant concentrations (30 min resolution) were obtained from the Neve Shaanan AQM station (marked AQM in Fig. 1), ~750 m down the road from site C (see below) and operated by the Haifa District Municipalities Association for the Environment (HDMAE). The AQM is located on the roof of a school, 10 m above the ground level (a.g.l.) and 30 m from the road, and it is considered by the HDMAE to be unaffected by local microenvironmental conditions. Ozone concentration measurements at the AQM station (O342M analyzer, Environment S.A. LTD, France; precision $\pm$ 0.5 ppb) were used as reference values for field calibration of the WDSN $O_3$ sensors. Wind data (30 min resolution) were also obtained from the AQM station.

### 2.2. Study area

The study area is the coastal city of Haifa, located at the eastern Mediterranean Sea at the north of Israel (~295,000 residents). The city is built on and around the Carmel Ridge, from the shore at the foot of the ridge to its top at ~400 m above sea level (a.s.l.). The campaign was done at Neve Shaanan — a residential neighborhood on the Carmel Ridge, ~200 m a.s.l. The neighborhood is mostly planar and features mixed residential and commercial areas. A major road crosses the neighborhood and connects the north-east and south-west slopes of the Carmel Ridge, passing through the Ziv junction — a neighborhood busy commercial area (Fig. 1). The summer along the Israeli coast of the Mediterranean, from mid-May to mid-October, is dominated by a Persian trough at the surface that is capped by an Azorean high aloft. This synoptic pattern results in rather stable hot and humid

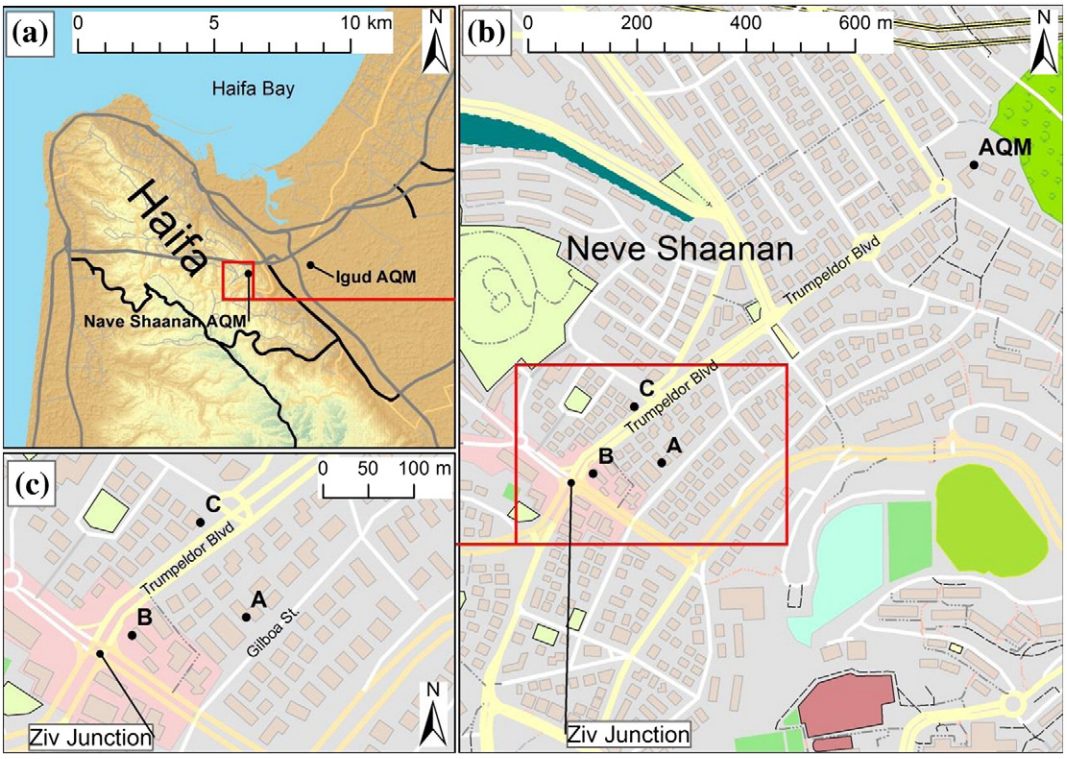


**Fig. 1.** Map of the study region showing the Haifa bay area and the Carmel Ridge (a), Neve Shaanan neighborhood (b) and the Ziv Junction area in greater detail (c).

meteorological conditions, with vigorous southwesterly winds during the day and a weak northeasterly land breeze at night.

### 2.3. Study design and site description

To test the sensors' response to different microenvironments at a neighborhood scale, six WDSN nodes were deployed at three different locations (two units per site) some 100–150 m apart (sites A, B and C, Fig. 1). The campaign took place for 71 days in the summer of 2013 (16/06/2013 to 26/08/2013). The units at site A were deployed on a balcony of a private apartment in a two-story building, 3 m a.g.l., facing a small street that is characterized by sparse traffic density (~5 m from the road). The units at site B were also deployed at a private balcony on the second floor of a two-story building, ~4 m a.g.l. The building is situated at the corner of the Ziv junction, 7 m off the adjacent busy street. The building's ground floor houses a pizzeria whose oven exhaust is at the rear side of the building. Site C is located at the main street of the neighborhood, ~80 m NE from a busy bus stop. The units were placed on a roof of a kindergarten courtyard, 3 m a.g.l. and 4 m off road.

Throughout the campaign, one unit was fixed at each site whereas the three remaining units were rotated twice between the sites, on days 28 and 51 from the beginning of the campaign. Therefore, these units operated at each of the three sites yet on different dates (Table 1). The rotation enabled the comparison of pollutant levels both within and between the sites, while still supporting scrutiny of each sensor's data quality. Due to the relatively stable meteorological conditions and emissions throughout the campaign, and following Hoek et al. (2008), we assumed that a period of 21–28 days is sufficient to characterize the pollution levels at each microenvironment.

Several options were studied for field calibration of the $O_3$ sensors. In particular, in the first trial the WDSN nodes were collocated at the Igud AQM station, which is located at the center of the Haifa Bay industrial-commercial area (marked Igud in Fig. 1a). The Igud AQM is situated on the roof of the HDMAE headquarters building, ~12 m a.g.l.

**Table 1**
Location of the WDSN nodes (identified by their 4XX serial code) during the three consecutive deployment periods.

| Location | Fixed node | Period I (Jun. 16–Jul. 14, days 1–28) | Period II (Jul. 14–Aug. 5, days 28–50) | Period III (Aug. 5–Aug. 26, days 50–71) |
|---|---|---|---|---|
| A | 418 | 422 | 413 | 424 |
| B | 420 | 424 | 422 | 413 |
| C | 414 | 413 | 424 | 422 |

## 3. Results and discussion

### 3.1. Inter-node consistency

In general, high correlations were found among measurements of collocated nodes during different time periods (Fig. 2). Specifically, the correlation coefficients and the mean absolute deviations between $O_3$, $NO_2$ and TVOC concentrations that were measured by collocated nodes did not differ significantly for different time-averaging periods (from 5 min to 1 day), suggesting consistency across WDSN measurements (Fig. S1 in the Supplementary information). Since 30 min. averaged concentrations are the highest reliable temporal resolution AQM data publically available in Israel, the Pearson's correlation coefficients, $r$, depicted in Fig. 2 are based on a comparable 30 min averaging of the WDSN nodes' measurements. Overall, the correlations range between 0.92 and 0.99 for $O_3$, 0.77 and 0.99 for TVOC and 0.78 and 0.98 for $NO_2$.

In contrast, low correlations are depicted between concentrations of both $NO_2$ and TVOC measured by WDSN nodes placed at different locations, indicating that the measured concentrations echoed to some extent local conditions and responded to the specific microenvironment where the nodes were placed. Similarly, Fig. 2a, d shows disparate

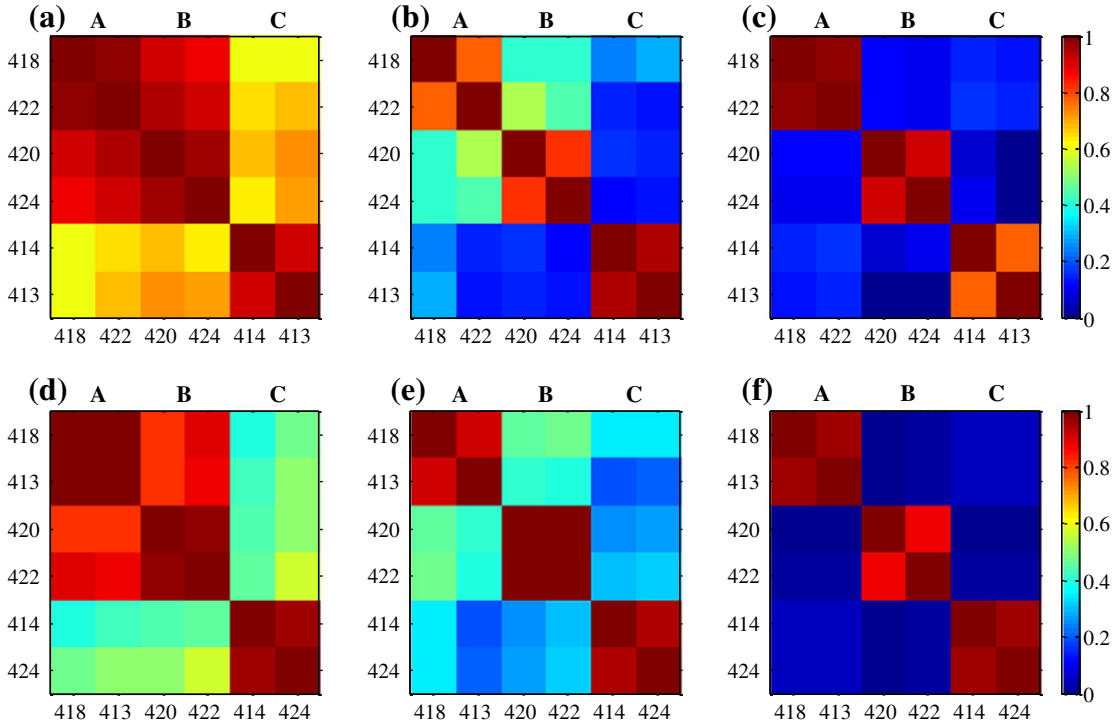


**Fig. 2.** Correlation coefficients of 30 min averaged concentrations during two time periods (Table 1): Period I (a)–(c) and Period II (d)–(f). $O_3$ (a) and (d), $NO_2$ (b) and (e), TVOC (c) and (f). Nodes deployment is presented in Table 1.

spatial behavior of the ozone correlation coefficients, with the concentrations measured at sites A and B highly correlated in both periods ($r = 0.82 - 0.94$) whereas lower correlations are revealed between the concentrations measured at either A or B and those measured at C, $r = 0.04 - 0.72$. It should be noted that observed urban ozone concentrations correspond to regional background concentration less the titrated ozone concentration as a result of local NO emissions (Seinfeld and Pandis, 2006). Since in urban areas NO emissions come almost solely from proximate vehicle traffic, the variability among the inter-site $O_3$ correlation coefficients suggests sensitivity of the sensors to local traffic conditions.

These results were consistent and the spatial pattern of the correlations remained unchanged irrespectively of the specific location of any individual node. For example, concentrations of $O_3$, $NO_2$ and TVOC measured by node 424 while at site B (period I) were highly correlated to the corresponding measurements of the collocated node 420 (Fig. 2a–c). However, when node 424 was moved to site C (period II) it showed almost no correlation to node 420 but was highly correlated with node 414, with whom it was collocated at site C (Fig. 2d–f). In general, Fig. 2 suggests that collocated WDSN nodes demonstrated good pollutant-specific inter-node correlation whereas nodes deployed at different locations, even within close proximity to each other, measured distinct concentrations that correspond to their disparate microenvironmental conditions. These results agree with our previous findings (Shashank et al., 2013) and suggest that AQ-WDSN could be used for measuring intra-urban (sub-neighborhood) pollutant variability.

### 3.2. Effect of deployment

Diurnal patterns of $NO_2$ concentrations among collocated AQ-WDSN nodes were similar (Fig. 3). In particular, after each rotation the $NO_2$ sensors successfully adjusted to their new microenvironments, measuring similar diurnal patterns to those reported by the fixed nodes (Fig. 3a, c). The weekday $NO_2$ daily patterns (Fig. 3a, c) reveal a distinct $NO_2$ signature in each site, with the patterns measured at site B showing typical morning and evening peaks (~70 ppb and ~50 ppb, respectively; Nazaroff and Alvarez-Cohen, 2001; Zalel et al., 2008; Levy, 2013). The diurnal patterns measured at site A, which is downwind of site B, were indeed similar to those measured at site B, but with much lower peak concentrations (25–30 ppb). In comparison, diurnal patterns measured at site C showed only a morning peak (70–95 ppb). During the weekend the daily peaks diminish and the diurnal patterns were similar at the three sites (Fig. 3b, d). This pattern results from the considerable decrease in traffic volumes in the Neve Shaanan neighborhood on Saturdays due to (a) a large community of religious residents who do not drive on Saturdays, (b) the halt of public transportation on Saturdays, and (c) the closing of most business in the commercial center on weekends. On Saturday afternoons (~17:00) $NO_2$ concentrations start to increase (especially at site B) since businesses reopen and traffic resumes. All these inner neighborhood patterns are nicely captured by the AQ-WDSN nodes.

Ambient $NO_2$ concentrations measured by the AQM station (dashed gray line in Fig. 3) were significantly lower than those concurrently measured by the WDSN nodes at the three sites. This discrepancy can result from higher concentrations at the AQ-WDSN sites, since they are much closer to the road than the AQM station. Alternatively, this discrepancy may partially result from an unsuitable (i.e. laboratory) calibration of the sensors by the manufacturer, which is not adequate for on-site urban conditions. Due to the low $NO_2$ concentrations measured at the AQM site during the study period (close to the sensors' detection limit — 10 ppb), field calibration of the $NO_2$ sensors (e.g. through collocation at the AQM site) could not be performed. Nonetheless, the weekday–weekend diurnal patterns (Fig. 3) demonstrate that the MO sensors can follow ambient $NO_2$ concentrations and that the WDSN nodes are sensitive to intra-urban pollutant variability.

In agreement with the results reported for $O_3$ and $NO_2$, measured TVOC concentrations also revealed high correlations between collocated nodes and microenvironment-specific diurnal patterns (Fig. 4). These results were consistent regardless of the site-specific node deployment (i.e. they were site specific rather than node specific; see node 424 in Fig. 4a, b). Furthermore, the diurnal and weekly patterns of TVOC concentrations at sites B and C were very similar to those of

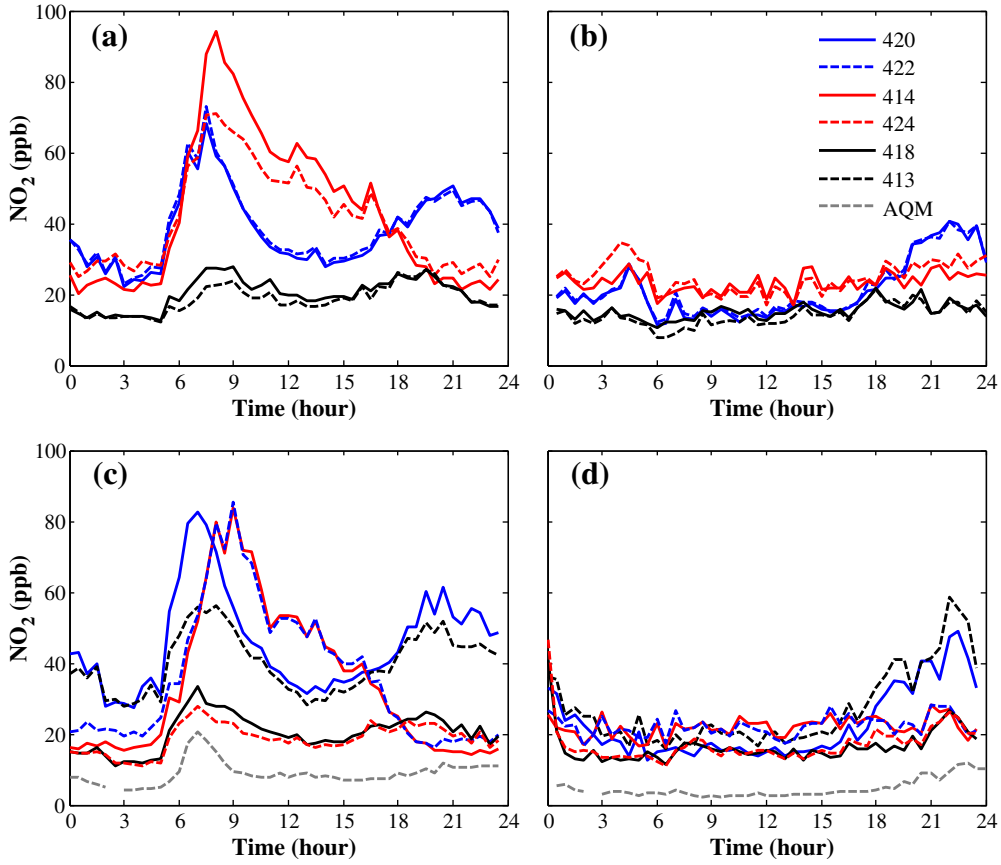


**Fig. 3.** Daily patterns of $NO_2$ concentrations (30 min averages) measured by collocated nodes in locations A (black lines), B (blue lines) and C (red lines) during Period II (plates a and b), and after the rotation (Period III, plates c and d). Left plates: measurements during weekdays (Sunday–Thursday), right plates: measurements during weekends (Saturdays). Dashed gray lines — simultaneous AQM monitoring data (available only during Period III).

the $NO_2$, suggesting that the TVOC sensors are sensitive to traffic-related pollution. Indeed, the two sites were deliberately chosen along a busy road section, and the TVOC concentrations (Fig. 4a, c) were within the reported range of urban CO concentrations (Mead et al., 2013; Carotta et al., 2001), suggesting that readings of the TVOC sensor were mostly due to ambient CO. Indeed, traffic related CO emissions are much higher than traffic related emissions of volatile organic pollutants (e.g. BTEX). In contrast, measured $NO_2$ concentrations at the residential site A were significantly lower than at sites B and C, and the TVOC patterns differed from those of the $NO_2$ (e.g. Fig. 4b). This implies a substantial contribution of non-traffic related local sources. It should be noted that field validation of the TVOC sensors by means of their deployment adjacent to an AQM station is impossible, since the AQM station used in this study does not monitor any VOCs.

### 3.3. Field calibration

Whereas measured ozone concentrations were highly correlated among collocated nodes (Fig. 2) they suffered from considerable inter-nodal variation, unlike the marginal inter-nodal variation of $NO_2$ and TVOC among collocated nodes. This inconsistency results from nodal-specific gain and bias that characterize the low-cost $O_3$ sensors. In a first trial to adjust the $O_3$ sensors all the nodes were placed adjacent to the Igud AQM station (Fig. 1a) for 20–50 days (between 27/12/2012 and 09/04/2013 and between 09/09/2013 and 13/10/2013) and their individual readings were compared to the reference $O_3$ measurements. High linear relationship ($r = 0.88$–$0.97$) was observed between the WDSN and the AQM measured $O_3$ concentrations, in agreement with Williams et al. (2013). Accordingly, using linear regressions, the nodes' measured $O_3$ values were adjusted to the AQM measurements. This adjustment improved considerably the inter-nodal measurement consistency, with the mean absolute error between the nodes decreasing from 4.3–17.1 ppb to 3.2–6.2 ppb. Yet, the individual nodes' gain and the bias coefficients were found to change significantly over time (Fig. 5). The temporal change of the regression coefficients can be attributed to aging of the sensors, resulting in alterations in the gain (Williams et al., 2013), and to episodic events, such as rain and dust storms, that cause dirt to accumulate on the sensors (Fig. 5c, d). The sensor-specific temporal variation of the calibration parameters results in a non-linear inter-nodal (i.e. relative) divergence of the readings and calls for a frequent field calibration of all the nodes. Since frequent collocation of the WDSN nodes with an AQM station is clearly impractical, a different method for field calibration was sought.

To this end, we propose a periodical calibration similar in principle to the calibration method of Tsujita et al. (2005) and based on the nearby AQM station data from 01:00–04:00 am. During this time period urban anthropogenic (i.e. local) emissions of $O_3$ precursors, namely $NO_2$ and TVOC, are negligible due to the cease of traffic and the absence of solar radiation. Hence, ozone production (due to photochemical reactions) and depletion (due to titration with fresh NO) are insignificant and $O_3$ concentrations tend to be relatively homogeneous and to reveal insignificant spatial variation at the urban residential neighborhood scale. Thus, we presumed that between 01:00 and 04:00 am the WDSN nodes in the Neve Shaanan neighborhood and the AQM station (deployed ~600–800 m away, Fig. 1b) report similar concentrations. A sensor-specific linear regression was developed (based on 30 min averages, to fit the temporal resolution of the AQM data) for each period (Table 1) and the regression coefficients were used for algorithmic

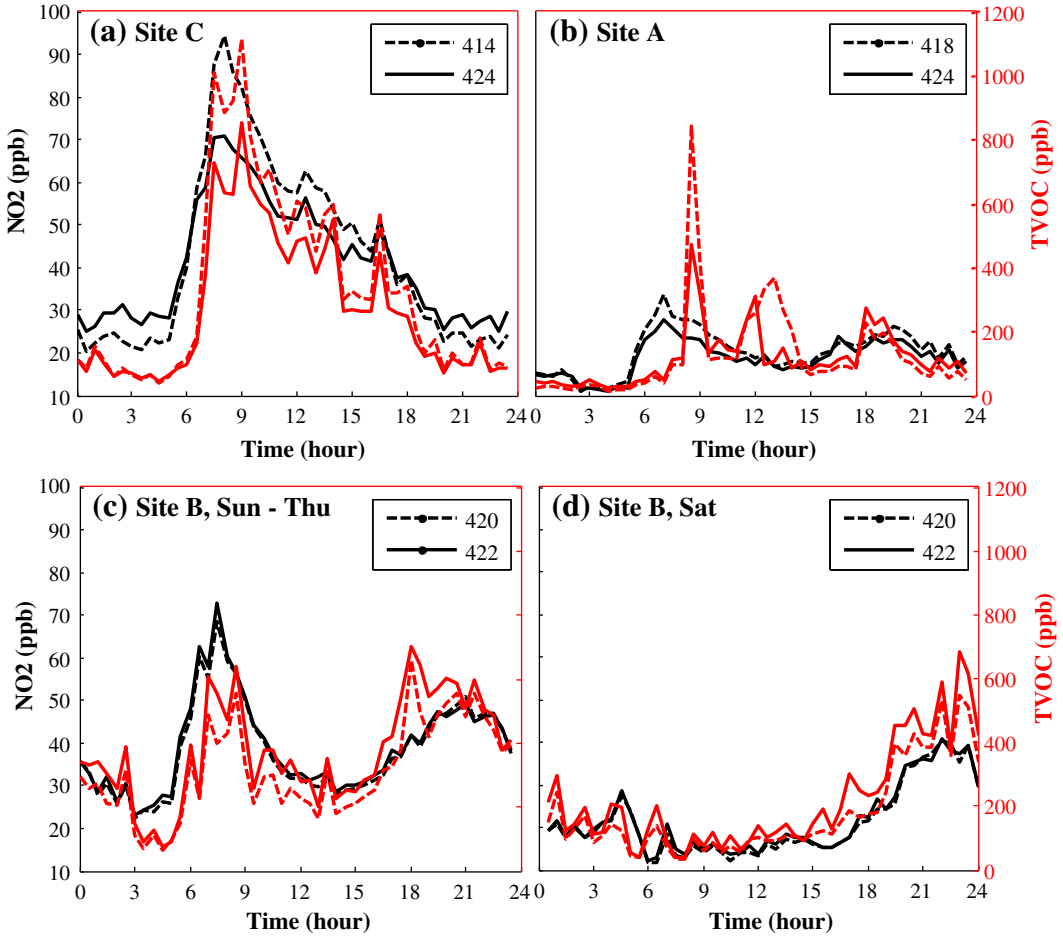


**Fig. 4.** Daily patterns of 30 min average $NO_2$ (black) and TVOC (red) concentrations at (a) site C during weekdays (Sunday–Thursday) on Period II, (b) site A during weekdays on Period III (to demonstrate the responsiveness of the TVOC sensor of node 424 to its new microenvironment), (c) site B during weekdays on Period II, and (d) site B during Saturdays on Period II. Solid and dashed lines correspond to different collocated nodes as specified.

adjustment of the sensor $O_3$ readings in the corresponding period, thus circumventing the effects of aging and general sensor degradation. This procedure was found to reduce the average mean absolute deviation between the collocated WDSN $O_3$ sensors from 13.3 (3.8–31.0) ppb to 1.3 (0.6–3.1) ppb.

Daily $O_3$ patterns at the three sites during weekdays (Sunday–Thursday) and weekends (Saturday) are depicted before and after the calibration adjustments (Fig. 6). The $O_3$ patterns (Fig. 6b, d) indicate that the in-situ night-time calibration procedure can overcome the disparity among ozone sensor measurements and bring them to a common ground (at night) while still revealing spatial variability during the day (resulting from traffic related emissions variability across the neighborhood). However, most neighborhoods within any city do not have an AQM station within their boundaries, whose data can be used as a reference value for such a calibration procedure. In such cases, rather than using AQM data we propose to use the 01:00–04:00 am mean value of all the nodes within the neighborhood. Whereas this procedure does not calibrate the sensors against true reference values, it does bring all the sensors to the same neighborhood-scale baseline, enabling to reveal the relative spatial variability of $O_3$ levels during the day (Fig. 6c, f) and reducing the mean absolute deviations among collocated sensors (0.7–3.7 ppb). The theoretical considerations underlying this field-calibration procedure are presented below.

### 3.3.1. Theoretical considerations

Let $\boldsymbol{y}_i$ and $\boldsymbol{Y_i}$ be pollutant measured time series, acquired at location $i$ by an WDSN node and by a standard AQM station, respectively. From the discussion in Section 3.3 and as illustrated in Fig. 5, $\boldsymbol{y}_i$ and $\boldsymbol{Y}_i$ are linearly connected, with $a_i$ and $b_i$ being the linear regression scalar coefficients,

$$\boldsymbol{y_i} = a_i \boldsymbol{Y_i} + b_i. \tag{1}$$

Clearly, when $\boldsymbol{Y_i}$ is unknown (e.g. when AQM station in not available at $i$) one cannot compute $a_i$ and $b_i$. Let $a_i$ and $b_i$ be the linear regression coefficients between $\boldsymbol{y}_i$ and the spatial mean of all nodes within a neighborhood, $\Omega$, at each time point during the night hours. The corrected value, $\hat{y}_i$, is

$$\hat{\boldsymbol{y}}_{\boldsymbol{i}} = \alpha_i \boldsymbol{y_i} + \beta_i. \tag{2}$$

Combining Eqs. (1) and (2),

$$\hat{y}_i = \alpha_i(a_i Y_i + b_i) + \beta_i = \alpha_i a_i Y_i + \alpha_i b_i + \beta_i. \tag{3}$$

Under the assumption of pollutant concentration homogeneity during the night hours, for any two locations $i, j \in \Omega$, $\boldsymbol{Y_i} = \boldsymbol{Y_j}$ and $\hat{y}_i = \hat{y}_j$. Hence,

$$\alpha_i a_i = \alpha_j a_j = A, \tag{4}$$

$$\alpha_i b_i + \beta_i = \alpha_j b_j + \beta_j = B. \tag{5}$$

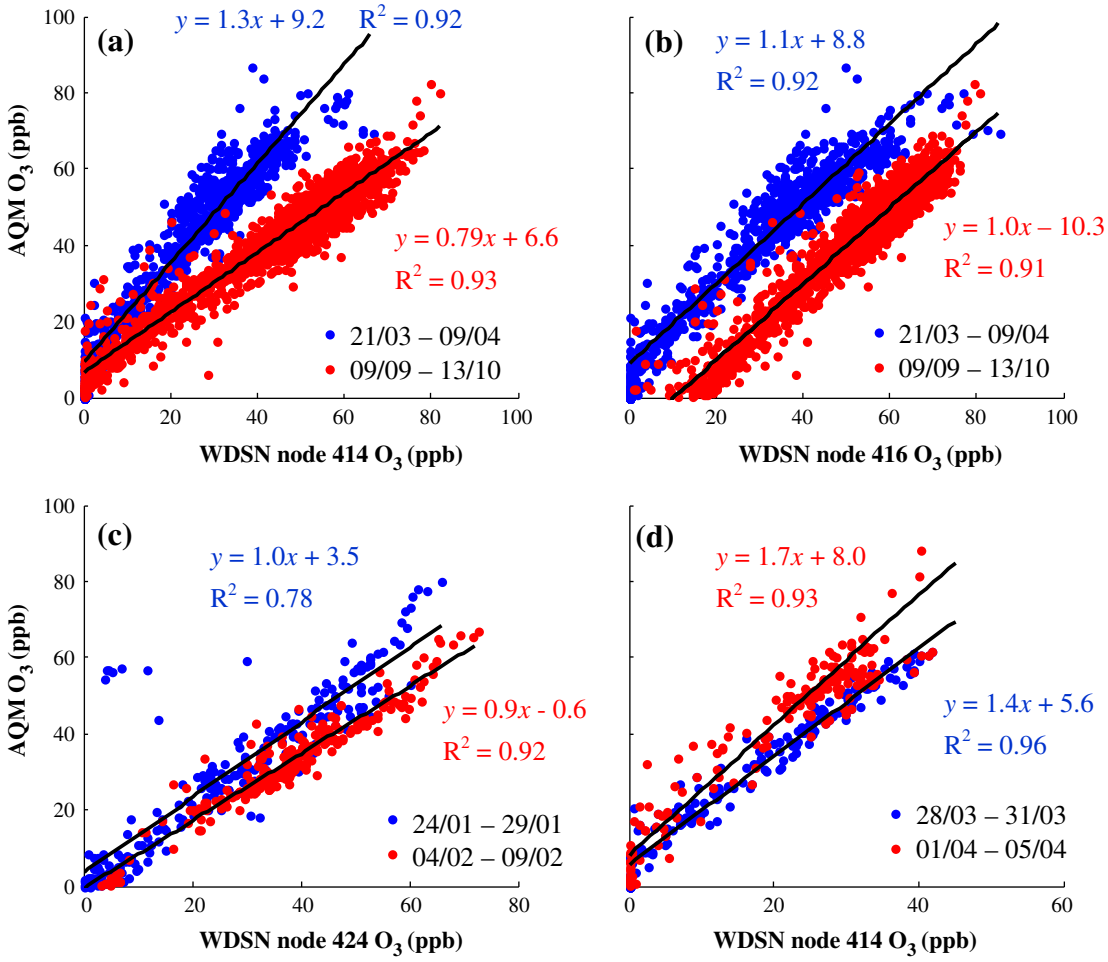


**Fig. 5.** Comparison of WDSN ozone measurements with AQM reference measurements performed at different periods during 2013 (30 min averages; typical examples). (a) Node 414, (b) node 416, (c) node 424 before (blue) and after (red) a rainy period, and (d) node 414 before (blue) and after (red) a dust event.

Rewriting Eq. (3) using Eqs. (4) and (5) results in

$$@i: \quad \hat{y}_i = A\boldsymbol{Y}_i + B. \tag{6}$$

Thus, for $A > 0$ it follows from (6) that the ratios $Y_i/Y_j$ and $\hat{y}_i/\hat{y}_j$ are consistent, i.e. they both are larger, equal or smaller than unity. Namely, the relative concentration ranking between any two sites (e.g. $\boldsymbol{Y_i} \gtrless \boldsymbol{Y_j}$) is maintained ($\hat{y}_i \gtrless \hat{y}_j$). Consequently, as long as the homogeneity assumption is valid, night time calibration to the mean value of all the nodes within the neighborhood provides a useful method for qualitative determination of locations with higher (lower) pollutant concentrations. As for quantitative interpretation of the data, when the actual concentration at location $i$ is λ times the actual concentration at site $j$, $Y_i = \lambda Y_j$, Eq. (6) results in

$$\hat{\boldsymbol{y}}_i = \lambda \hat{\boldsymbol{y}}_j + (1-\lambda)B. \tag{7}$$

Alternatively, when $Y_i = Y_j + \mu$ Eq. (6) results in

$$\hat{\boldsymbol{y}}_i = \hat{\boldsymbol{y}}_j + A\mu. \tag{8}$$

As evident from Eqs. (7)–(8), the calibrated concentrations generally do not preserve the ratio (λ) or the difference ($\mu$) between the actual concentrations at different locations but when $B \approx 0$ or $A \approx 1$, respectively. It is noteworthy that our measurements suggest that $A \sim 1$ (Fig. 5). Hence, the differences in ozone concentrations measured at different locations by the WDSN nodes following calibration to the mean nighttime neighborhood AQM data correspond closely with the true spatial concentration differences. Further research is required to assess the propagation of errors generated by the two proposed field calibration procedures.

### 3.3.2. Semi-continuous predictive field-calibration

The regression coefficients of the two field calibration procedures proposed above were calculated based on all the data points between 01:00 and 04:00 of the relevant study period. However, it is possible to apply these procedures also in a predictive mode, i.e. with the calibration coefficients for each day calculated based on the 01:00–04:00 data from the same day or from a few previous days. Since the WDSN data available for us do not cover a sufficiently long period, we present here only preliminary results that demonstrate the concept using 5 min averaged AQM data. Fig. 7 depicts changes in the regression slope, intercept and $R^2$ as a function of the number of nights (i.e. data points) used. As seen, whereas data from one night is insufficient for obtaining reliable regression parameters they tend to stabilize using data from 2 to 4 nights (Fig. 7b–d). Using data from longer periods seems to introduce disturbances and deteriorate the results, in accordance with Fig. 5c of Yuval and Broday (2010), where ozone concentrations from periods longer than 4 days are shown to be uncorrelated. Therefore, calibration coefficients for each day were calculated based on AQM data from 1:00 to 4:00 am of the three preceding days. This rolling forwards field calibration procedure reduced the average mean

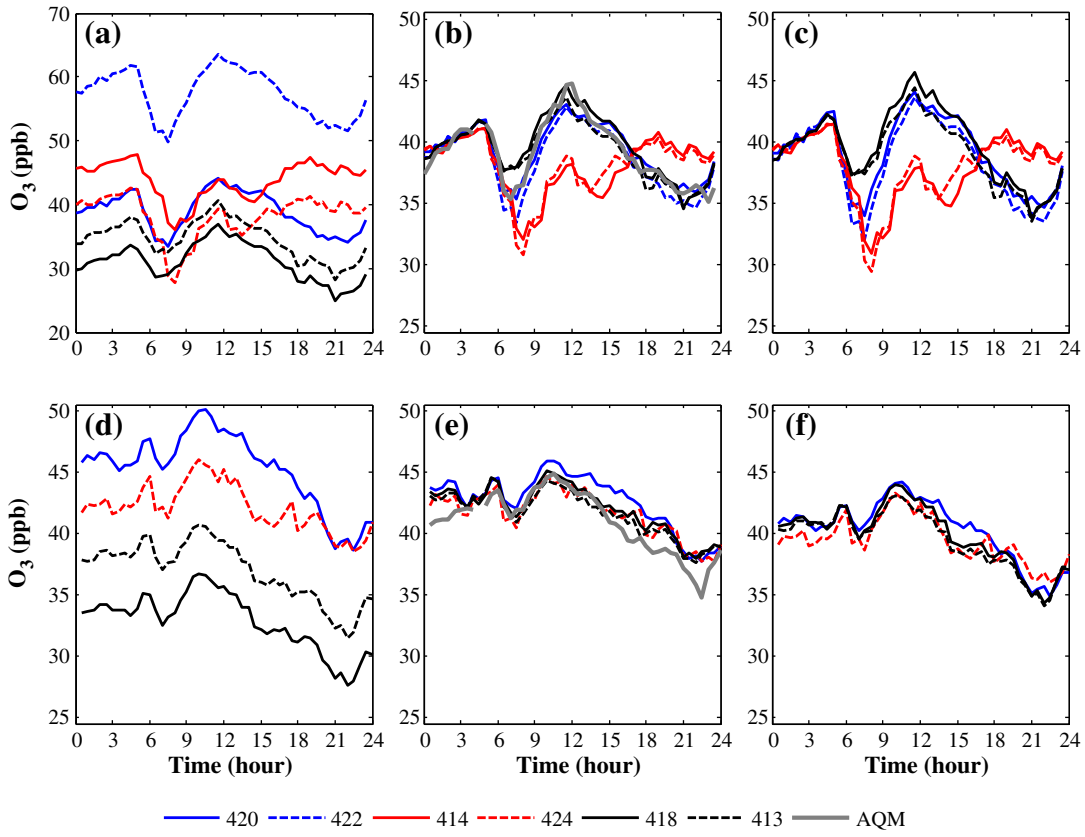


**Fig. 6.** Daily patterns of 30 min average $O_3$ concentrations in Period II during weekdays (Sunday–Thursday; upper row) and Saturdays (lower row) before calibration (a and d), after calibration based on AQM data from 1:00–4:00 am (b and e), and after calibration based on the mean 1:00–4:00 am value of all the WDSN nodes in the neighborhood (c and f). The $O_3$ sensors of nodes 414 and 422 stopped working on day 38, therefore the patterns shown in plates a–c are based only on data from days 28–38. Nodes' deployment is presented in Table 1.

absolute deviation between collocated WDSN $O_3$ measurements from 3.7–18.7 ppb to 0.5–1.1 ppb, and enabled revealing the spatial variability of daily $O_3$ concentrations (Fig. 7a).

It is noteworthy that the concept behind the proposed field-calibration procedures can be applied to other air pollutants as long as they exhibit negligible spatial variation for a sufficiently long period, provided that the true concentrations are above the sensors' detection limit. Unfortunately, this criterion did not hold for $NO_2$ in this study.

### 3.4. Sensitivity to microenvironmental conditions

The capability of WDSN nodes to perceive pollutants' spatial variability at the neighborhood scale has been demonstrated (Figs. 2–4). In particular, although the three sites are located only ~100–150 m apart, they are readily distinguishable based on the AQ-WDSN measurements. For example, site A is located in a small residential street with little traffic and is characterized by lower $NO_2$ and TVOC concentrations than the two other sites (Figs. 3a, c and 4b). Nevertheless, weekday $NO_2$ concentrations at site A exhibit a typical traffic related diurnal pattern with a morning (7:00–7:30) and an evening (~19:30) rush hour peaks (Fig. 3a, c). In contrast, TVOC concentrations reveal a different daily pattern (Fig. 4b) with the higher TVOC concentrations approaching site A from different directions than the higher $NO_2$ concentrations (Fig. S2 in the Supplementary information). This suggests that TVOC concentrations at site A originate, at least partially, from non-traffic sources. In fact, the bivariate $NO_2$ and TVOC polar plots (Fig. S2) demonstrate very effectively the site-specific disparate air quality measurements by the WDSN nodes.

Site B is located at a busy junction in a commercial area. Indeed, the diurnal patterns (Fig. 4) and to a smaller extent the bivariate plot (Fig. S2) are similar for both pollutants, suggesting that they emanate from the same sources. Whereas on weekdays both $NO_2$ and TVOC reveal a dual-peak daily pattern (Figs. 3a, c and 4c), on Saturdays the concentrations remain low and constant until ~19:00, when traffic resumes (Figs. 3b, d and 4d). The signature of traffic is revealed also in the weekday ozone concentration patterns, which show a dramatic decrease from 05:30 am and reach a minimum at about 07:00–07:30, in parallel to the $NO_2$ peak (Fig. 4c). Typically, $O_3$ concentrations increase more slowly and reach peak values at around noon (Fig. 6). It is noteworthy that the highest $NO_2$ and TVOC concentrations were measured when the wind blew from N-NW or when the wind speed was in general relatively low (<3 m/s, Fig. S2). This probably reflects the contribution of local sources (mainly traffic) but may also demonstrate the effect of in-situ emissions of the pizzeria (in the rear of the building), which are dispersed efficiently when stronger winds were blowing (from the SW).

Likewise, the weekday daily patterns of both $NO_2$ and TVOC (Fig. 4a) and the bivariate plots (Fig. S2) at site C indicate traffic related origin. Peak $NO_2$ and TVOC concentrations and minimum $O_3$ concentrations occurred at 08:00–09:00 am (Figs. 4a, c and 6b), somewhat later than at the two other sites. This could be possibly attributed to children drop off at the kindergarten. During the morning hours, the low mean wind speed (Fig. 8a) and the high traffic volume at the Ziv junction result in high concentrations at both B and C (Fig. 9a). Both Fig. 8 and the bivariate plots (Fig. S2) suggest that the highest pollutant concentrations in C are observed when the wind blows along the Trumpeldor Blvd. from the Ziv junction and the nearby bus stop, i.e. channeled along the urban land cover. In the afternoon, reduced traffic volume and higher wind speeds (Fig. 8b) result in significantly lower concentrations at site B (Fig. 9d) whereas site C maintains its relatively higher

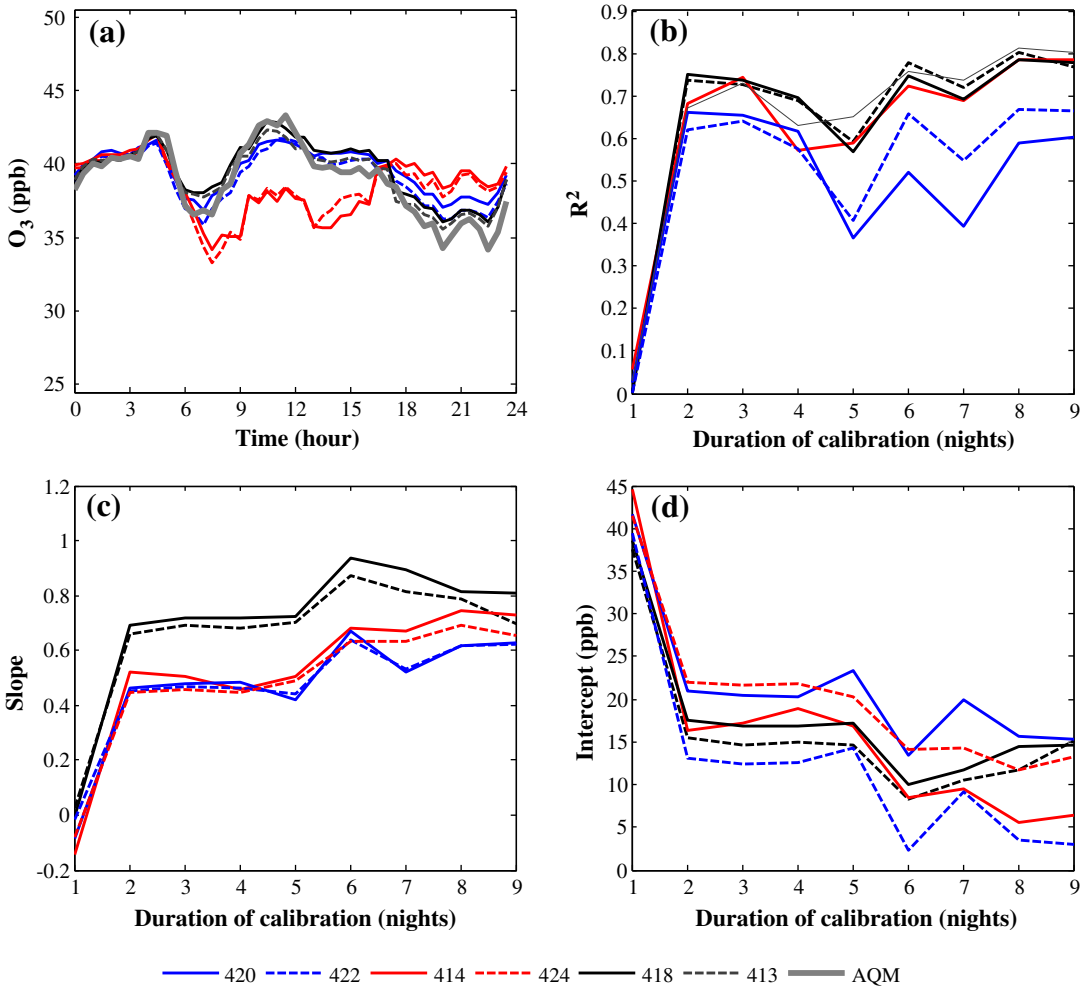


**Fig. 7.** Daily patterns of 30 min average $O_3$ concentrations in Period II during weekdays (Sunday–Thursday) after daily calibration based on AQM data from 1:00–4:00 am of the three previous days (a), and variation of the coefficient of determination of the regression, $R^2$, (b) and of the regression slope (c) and intercept (d) with the calibration duration.

concentrations (Figs. 3a, c, 4a and 9c). It is noteworthy that no evening rush hour peak is evident in the $NO_2$ and TVOC concentrations at site C, possibly since at that time the kindergarten is already closed and the evening westerly winds (Fig. 8c) diminish the impact of the nearby bus stop (Figs. 3a, c, 4a and 9e). In contrast, site B is affected in the evening by the now upwind bus stop at the Trumpeldor Blvd. (Fig. 9f). The effect of the bus stops on sites B and C, as described above, is consistent with previous studies that reported high $NO_2$ concentrations near bus

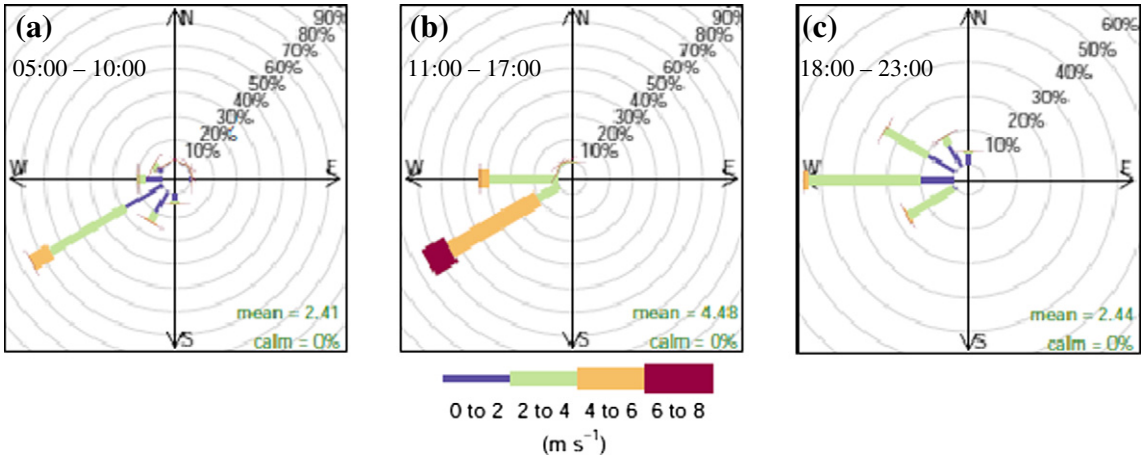


**Fig. 8.** Wind rose plots based on data measured at the AQM station on Period I. (a) Morning, (b) noon and afternoon, and (c) evening.

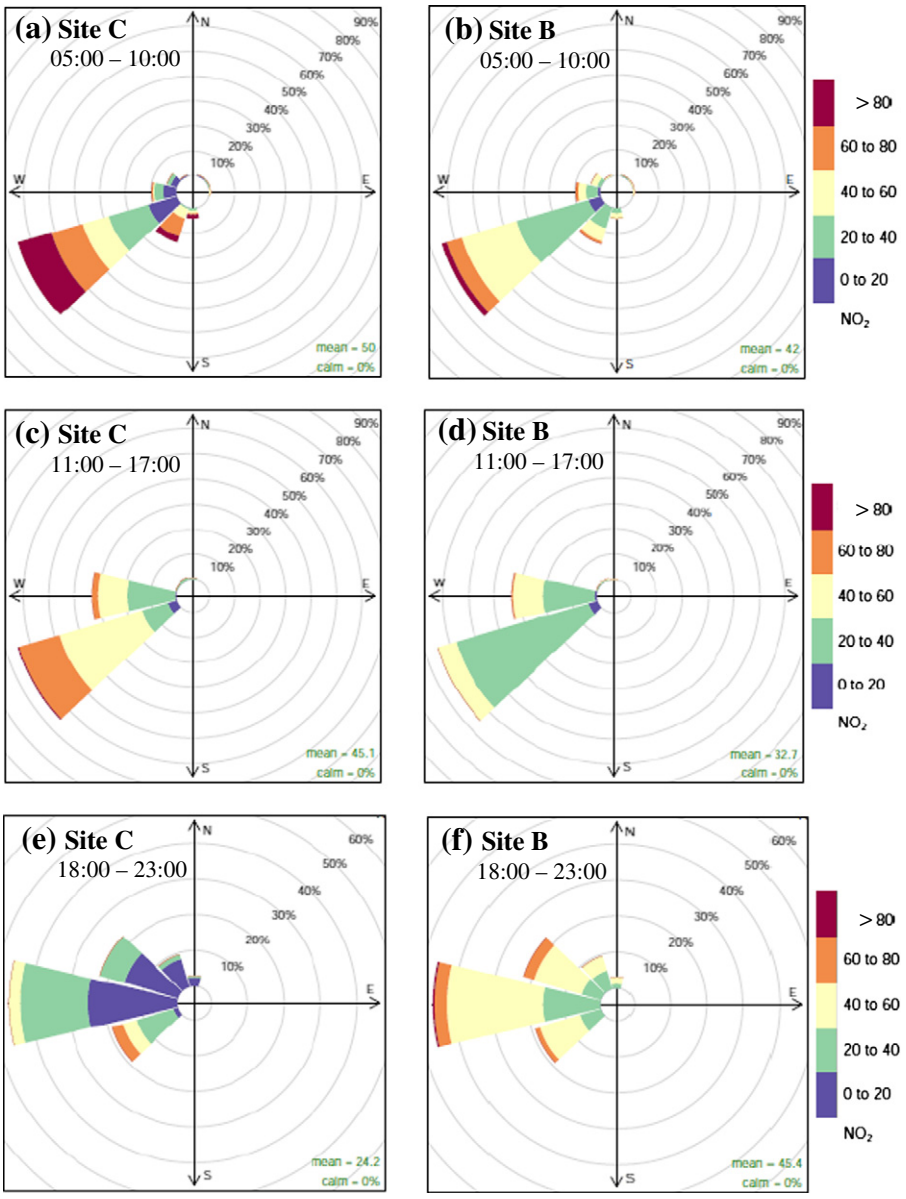


**Fig. 9.** Pollution rose plots of 30 min average $NO_2$ concentrations from Period I. Left — site C, right — site B. Upper row — morning, middle row — noon and afternoon, bottom row — evening. The wind data were taken from the nearby AQM station.

stops (Ahmad and Aziz, 2013) and could be studied only using very high node density. The latter has been demonstrated in this study using only 3 dual-node AQ-WDSN sites deployed in very close proximity to each other. Clearly, the full capabilities of this technology, including identification and characterization of common residential neighborhood sources, can be revealed only when deploying a larger network over a larger area.

In summary, we showed that it is possible to identify intra-urban pollutant "hot-spots" based on WDSN measurements. The similarity among the concentration patterns during Saturdays at the three sites (Figs. 4e and 6e) further support our conclusion that the nodes are very sensitive and respond instantaneously to their microenvironment local conditions.

## 4. Conclusions

We have demonstrated the suitability of metal-oxide WDSN for measuring urban air pollutant levels and for capturing their spatiotemporal concentration variability at the neighborhood scale. The WDSN nodes revealed high inter-node consistency and sensitivity to their microenvironment local conditions, making it possible to identify intra-urban pollutant "hot-spots". To reduce the considerable inter-nodal variation of measured ozone concentrations, a field calibration by a collocated reference instrument was performed. Although this procedure improved considerably the inter-nodal measurement consistency, sensor-specific temporal variation of the calibration parameters was observed, resulting in a non-linear inter-nodal (i.e. relative) divergence of the readings. Therefore, a periodical calibration based on the nearby AQM station nighttime data was proposed. This procedure was found to reduce the spread of readings by the nearby deployed sensor nodes, circumventing the effects of aging and general sensor degradation. Hence, the use of AQ-WDSN has a huge potential for providing intra-urban concentrations of airborne pollutants at an unprecedented resolution, capturing their fine and dynamic spatial variability at a very high temporal resolution. As such, AQ-WDSNs have a great potential to become a common tool in exposure and environmental epidemiology studies.

## Acknowledgment

This work was partially supported by the German-Israeli Foundation for Scientific Research and Development (GIF) (grant no. 2301-2296.10) Young Scientist Program, the Environment and Health Fund (Israel) Grant Award no. RPGA 1201, the 7th European Framework Program (FP7) ENV.2012.6.5-1, grant agreement no. 308524 (CITI-SENSE), and the Technion Center of Excellence in Exposure Science and Environmental Health (TCEEH).

## Appendix A. Supplementary data

Supplementary data to this article can be found online at http://dx.doi.org/10.1016/j.scitotenv.2014.09.059.

## References

Ahmad S, Aziz N. Spatial and temporal analysis of ground level ozone and nitrogen dioxide concentration across the twin cities of Pakistan. Environ Monit Assess 2013;185(4):3133–47.
Becker T, Muhlberger S, van Braunmuhl CB, Muller G, Ziemann T, Hechtenberg KV. Air pollution monitoring using tin-oxide-based micro-reactor system. Sensors Actuators B 2000;69:108–19.
Carotta M, Martinelli G, Crema L, Malagu C, Merli M, Ghiotti G, et al. Nanostructured thick-film gas sensors for atmospheric pollutant monitoring: quantitative analysis on field tests. Sensors Actuators B 2001;76:336–42.
Crouse DL, Goldberg MS, Ross NA. A prediction-based approach to modelling temporal and spatial variability of traffic-related air pollution in Montreal, Canada. Atmos Environ 2009;43(32):5075–84.
Eitan O, Yuval, Barchana M, Dubnov J, Linn S, Carmel Y, et al. Spatial analysis of air pollution and cancer incidence rates in Haifa bay, Israel. Sci Total Environ 2010;408:4429–39.
Hoek G, Beelen R, de Hoogh K, Vienneau D, Gulliver J, Fischer P, et al. A review of land-use regression models to assess spatial variation of outdoor air pollution. Atmos Environ 2008;42:7561–78.
Kampa M, Castanas E. Human health effects of air pollution. Environ Pollut 2008;151(2):362–7.
Kanaroglou P, Jerrett M, Morrison J, Bernardo Beckerman M, Arain A, Gilbert N, et al. Establishing an air pollution monitoring network for intra-urban population exposure assessment: a location-allocation approach. Atmos Environ 2005;39(13):2399–409.
Lee D. Environmental gas sensors. IEEE Sensors J 2001;1(3):214–24.
Levy I. A national day with near zero emissions and its effect on primary and secondary pollutants. Atmos Environ 2013;77:202–12.
Levy I, Mihele C, Lu G, Narayan J, Hilker N, Brook J. Elucidating multipollutant exposure across a complex metropolitan area by systematic deployment of a mobile laboratory. Atmos Chem Phys 2014a;14:1–21.
Levy I, Mihele C, Lu G, Narayan J, Brook JR. Evaluating multipollutant exposure and urban air quality: pollutant interrelationships, neighborhood variability, and nitrogen dioxide as a proxy pollutant. Environ Health Perspect 2014b;122(1):65–72.
Mead M, Popoola O, Stewart G, Landshoff P, Calleja M, Hayes M, et al. The use of electrochemical sensors for monitoring urban air quality in low-cost, high-density networks. Atmos Environ 2013;70:186–203.
Myers V, Broday DM, Steinberg DM, Yuval, Drory Y, Gerber Y. Exposure to particulate air pollution and long-term incidence of frailty after myocardial infarction. Ann Epidemiol 2013;23(7):395–400.
Nazaroff W, Alvarez-Cohen L. Environmental Engineering Science. New-York, NY: John Wiley; 2001.
Peters A, Döring A, Wichmann H, Koenig W. Increased plasma viscosity during an air pollution episode: a link to mortality? Lancet 1997;349(9065):1582–7.
Piedrahita R, Xiang Y, Masson N, Ortega J, Collier A, Jiang Y, et al. The next generation of low-cost personal air quality sensors for quantitative exposure monitoring. Atmos Meas Tech Discuss 2014;7:2425–57.
Pope CA, Burnett RT, Thun MJ, Calle EE, Krewski D, Ito K, et al. Lung cancer, cardiopulmonary mortality, and long-term exposure to fine particulate air pollution. JAMA 2002;287(9):1132–41.
Pujades-Rodríguez M, McKeever T, Lewis S, Whyatt D. Effect of traffic pollution on respiratory and allergic disease in adults: cross-sectional and longitudinal analyses. BMC Pulm Med 2009;9(42):1–11.
Rao S, Chirkov V, Dentener F, Dingenen R, Pachauri S, Purohit P, et al. Environmental modeling and methods for estimation of the global health impacts of air pollution. Environ Model Assess 2012;17(6):613–22.
Seinfeld JH, Pandis SN. Atmospheric chemistry and physics: from air pollution to climate change. 2nd ed. New York, NY: J. Wiley; 2006.
Shashank J, Levy I, Fishbain B, Broday DM. Application of distributed sensor networks for estimating exposures to air pollution in urban areas. The Annual Conference of ISEE, ISES and ISIAQEnvironment and health — bridging south, north, east and west; 2013. [Basel, Switzerland].
Tsujita W, Yoshino A, Ishida H, Moriizumi T. Gas sensor network for air-pollution monitoring. Sensors Actuators B 2005;110:304–11.
Whitworth K, Symanski E, Lai D, Coker A. Kriged and modeled ambient air levels of benzene in an urban environment: an exposure assessment study. Environ Health 2011;10:21–30.
Williams D, Henshaw G, Bart M, Laing G, Wagner J, Naisbitt S, et al. Validation of low-cost ozone measurement instruments suitable for use in an air-quality monitoring network. Meas Sci Technol 2013;24(6):5803–14.
Yuval, Broday DM. High resolution spatial patterns of long-term mean air pollutants concentrations in Haifa Bay area. Atmos Environ 2006;40(20):3653–64.
Yuval, Broday DM. Studying the time scale dependence of environmental variables predictability using fractal analysis. Environ Sci Tech 2010;44(12):4629–34.
Zalel A, Yuval, Broday DM. Revealing source signatures in ambient BTEX concentrations. Environ Pollut 2008;156(2):553–62.